INTERNATIONAL TABLES FOR CRYSTALLOGRAPHY

ISSN 1574-8707
it.iucr.org

Volume I, X-ray Absorption Spectroscopy
and Related Techniques
ISBN: 978-1-119-43394-1

Chapter 3.4

Bragg crystal monochromators

John P. Sutter*

Diamond Light Source Ltd, Harwell Science and Innovation Campus, Chilton, Didcot OX11 0DE, United Kingdom.
*Correspondence e-mail: john.sutter@diamond.ac.uk

Materials that have been used in Bragg crystal monochromators for EXAFS studies are examined and compared. Current designs of single-crystal and multi-crystal monochromators are described, and the trends affecting their future development are discussed.

Keywords: monochromators for EXAFS; energy resolution; Bragg reflections; rocking curve; Darwin width.

Related chapters
Volume I: 3.5, 3.7

1. Introduction

Once X-rays have been produced, whether by a small laboratory device such as a tube or plasma, or by a large machine like a synchrotron or free-electron laser, they must be processed by a set of optical components into a form suitable for the desired experiment. Diffraction gratings, multilayers and crystals perform the common yet critical task of selecting X-rays of a particular energy. Such optical components are monochromators. A monochromator is chosen according to the range of X-ray energies E it can select, the bandwidth ΔE about the selected energy, and the efficiency with which it transmits X-rays of the selected energy and blocks X-rays of all other energies. Monochromator designs for EXAFS must furthermore maintain an accurate energy calibration and must keep the exiting beam's intensity, position and angle stable while scanning over the X-ray energy. This distinguishes EXAFS monochromators from those used for imaging or macromolecular crystallography, which are normally carried out at a fixed X-ray energy.

Bragg reflections from crystals are the most common way to select X-ray energies above 5 keV, where they are highly efficient. While multilayers provide a relative bandwidth $\Delta E/E \simeq 10^{-2}$ in this range, crystals can achieve $\Delta E/E \simeq 10^{-4}$. Some crystals can even select X-ray energies down to 1 keV, where diffraction gratings become competitive. Crystals are essentially three-dimensional diffraction gratings of atomic scale, because the size of an atom is several ångströms, comparable to an X-ray wavelength. They may be treated as sets of planes of atoms separated by a uniform spacing d, with each plane reflecting a very small fraction of the incident X-ray wave. If the X-rays form a plane wave of wavelength λ making an angle θ with the planes of atoms, the reflected waves from all the planes of atoms interfere constructively and hence yield a large total reflected intensity if Bragg's law is fulfilled:

$$2d\sin\theta = n\lambda, \tag{1}$$

where n is a positive integer called the 'order.' (A small refractive correction to θ is neglected here.) Crystal monochromators thus transmit integer multiples ('harmonics') of the selected X-ray energy, and different methods are used to suppress them, such as the detuning of the monochromator or the use of harmonic rejection mirrors. This is critical for X-ray absorption spectroscopy beamlines.

2. Crystal types and symmetries

A crystal is classified according to its space group, which is the set of rotations, reflections, inversions, translations and combinations of these that transform the crystal structure into itself. Every crystal structure belongs to exactly one of the 230 three-dimensional space groups gathered into one of fourteen Bravais lattices. These in turn are classified under seven crystal systems, listed as follows from most to least symmetric: cubic, tetragonal, hexagonal, trigonal (rhombohedral), orthorhombic, monoclinic and triclinic. The properties of the individual crystal systems and space groups are provided in *International Tables for Crystallography* Volume A (2016), but a few of the most important ones will be reviewed here. A thorough discussion of these concepts may also be found in Ashcroft & Mermin (1976).

The scattering from a unit cell of a crystal is described by Cullity & Stock (2001). Each set of planes within a crystal is assigned a set of three Miller indices hkl that are inversely proportional to the intercepts of the plane through the basis vectors $\mathbf{a}$, $\mathbf{b}$ and $\mathbf{c}$. If the unit cell is hexagonal, as is usually the case for trigonal as well as hexagonal crystals, a plane is assigned four Miller–Bravais indices $hkil$, where $i = -(h + k)$, in order to clarify the equivalence of symmetry-related planes about the c axis. The normal to the (hkl) plane lies along the scattering vector $\mathbf{G}_{hkl}$, which is always equal to the wavevector of the diffracted beam minus that of the incident beam when the Bragg condition in equation (1) is fulfilled. In order for a set of planes to produce a Bragg reflection, their Miller or Miller–Bravais indices must all be integers, and must also satisfy relationships imposed by the symmetry operations of the crystal's space group. These emerge from the calculation of the scattering amplitude, or 'structure factor' F_{hkl} of the unit cell for scattering from the (hkl) planes. If the unit cell contains N atoms, the structure factor neglecting temperature corrections is

$$F_{hkl} = \sum_{j=1}^{N} f_j(\mathbf{G}_{hkl}) \exp\left(2\pi i \mathbf{G}_{hkl} \cdot \mathbf{r}_j\right), \qquad (2)$$

where $\mathbf{r}_j = x_j\mathbf{a} + y_j\mathbf{b} + z_j\mathbf{c}$ is the position of the jth atom within the unit cell. Note that $0 \le x_j, y_j, z_j < 1$ for all j. f_j is the scattering amplitude, or 'atomic form factor,' of the jth atom. It depends on the detailed distribution of the electrons around the jth atom's nucleus. If all atoms in the crystal are identical, then it is especially easy to see from this equation that some planes (hkl) produce Bragg reflections while others do not. For instance, if that crystal's lattice is body-centred, it has Bragg reflections only from planes for which $h + k + l$ is even, and if the lattice is face-centred, it has Bragg reflections only from planes for which h, k and l are either all even or all odd. Further conditions can be found in *International Tables for Crystallography*, Volume A, in the 'Positions' part of the table for the crystal's space group. For example, three crystal materials widely used as X-ray monochromators, namely silicon, diamond and germanium, belong to the same face-centred cubic space group $Fd\bar{3}m$ and have their atoms at Wyckoff positions $8a$. The general and special conditions together can be summarized as hkl all odd, or hkl all even and $h + k + l$ a multiple of 4.

The less symmetry a crystal's space group has, the less likely it becomes that one particular atomic plane of that crystal will be symmetry-equivalent to any other. For example, in crystals that form cubic lattices of the space group $Fd\bar{3}m$, the set of symmetry-related atomic planes $\{hkl\}$ may contain up to 48 members unless two or more of the Miller indices are equal. On the other hand, in α-quartz, whose lattice is trigonal and which can exist in either of two enantiomorphic space groups $P3_121$ or $P3_221$, the set of symmetry-related atomic planes $\{hkl\}$ can contain no more than six members. A crystal lattice of the centrosymmetric triclinic space group $P\bar{1}$, which includes only inversion centres and translations along the basis vectors $\mathbf{a}$, $\mathbf{b}$ and $\mathbf{c}$ among its symmetry operations, would have only the two planes (hkl) and $(\bar{h}\bar{k}\bar{l})$ as members of $\{hkl\}$. In the extreme example of a crystal of the triclinic space group $P1$, every atomic plane is unique because such a crystal remains invariant only under translations along its basis vectors $\mathbf{a}$, $\mathbf{b}$ and $\mathbf{c}$. Table 3.2.3.2 in *International Tables for Crystallography* Volume A lists the members of the sets of symmetry-equivalent atomic planes $\{hkl\}$ for the 32 crystallographic point groups. For each of the 230 crystallographic space groups, there is exactly one such point group. See Section 1.3.3.1 in *International Tables for Crystallography* Volume A (2016) for details. The number of Bragg reflections within a given range of X-ray energies that have distinct interplanar spacings and structure factors therefore depends critically on the degree of symmetry of the crystal's space group.

3. Material properties of crystals

However, the suitability of a particular crystal for use as an X-ray monochromator depends on much more than just its space group. The crystal's material properties also play an important role.

First, the crystal must be able to withstand the X-ray photon flux without suffering excessive damage during the time of the experiment. Many crystals can be chosen for the collection and analysis of X-ray fluorescence, which is of low intensity and spread over a wide range of solid angles. On the other hand, only a few crystals, particularly silicon and diamond, can endure the high and concentrated X-ray flux generated by a synchrotron source. This requirement in itself limits the usefulness of crystals for selecting X-rays of energy below about 2 keV, because the crystals that offer planes of suitably large d-spacing tend to be composed of large organic molecules (for example, acid phthalates) that degrade easily when irradiated. Among the few exceptions are beryl, which is rare, and YB_{66}, an artificial, very complex cubic crystal with over 1600 atoms in each unit cell. Both of these materials were once considered for use in monochromators at synchrotron beamlines (Wong *et al.*, 1999), but are rarely used there today for reasons that will become clear in the following.

Second, although ideal crystals have been discussed in the previous section, real crystals fall short of perfection in different ways and to varying degrees depending on the conditions in which they were grown, even if great care is taken to make them chemically pure. Dislocations are very common and can lead to stacking faults and grain boundaries, which can broaden the energy resolution and alter the flux diffracted by the crystal. At one extreme there is silicon, which can be grown in large, highly pure, dislocation-free ingots by the float-zone method. Diffraction from such large, perfect crystals must be treated by dynamical diffraction theory, which accounts for the mutual coupling between the incident and diffracted waves within the crystal (Batterman & Cole, 1964). Perfect crystal monochromators provide the minimum possible bandpass. They also provide the highest diffraction efficiency, but the divergence they can accept is very small ($\sim$10 μrad) unless the Bragg angle deviates from 90° by less than a few tenths of a degree. Perfect crystals are required when the thermal and mechanical properties of a monochromator must be spatially uniform and well characterized, for example when subjected to the high power load of a synchrotron beamline, or when elastically bent [*e.g.* PET, Källne & Källne (1983); quartz, silicon and germanium, Pattison *et al.* (1986)]. At the other extreme, many real crystals can be analysed as mosaic structures composed of many small, perfect crystal blocks that are slightly misaligned with respect to one another and scatter independently. Zachariasen (1945) provides detailed calculations of diffracted intensities from such crystals. Mosaic crystals diffract less efficiently than perfect crystals and their spatial properties are generally not uniform, but this can be compensated by the mosaic crystals' increased angular acceptance. Ice & Sparks (1990) showed that a sagitally curved graphite mosaic crystal spectrometer brought more flux to the detector than a perfect crystal while maintaining a similar energy resolution. On the other hand, the strong mosaicity in even the best synthetically grown diamond crystals has limited their application as monochromators of high-intensity synchrotron X-ray beams despite diamond's excellent thermal conductivity, which is discussed below. Other materials lie between these two extremes. For example, the best sapphire crystals now available show variations in strain on the scale of tenths of millimetres (Sergueev *et al.*, 2011) and a significant concentration of dislocations (Asadchikov *et al.*, 2016), but these did not prevent their use as high-resolution monochromators as long as the incident beam was confined to a small region ($\sim$1 mm^2) of the crystal. Lithium niobate crystals grown by the usual Czochralski method suffer from compositional gradients, dislocations and subgrain boundaries; attempts to improve them are ongoing (Sarker, 2016). Quartz in nature is well known for its various types of twinning, but synthetically grown quartz crystals can be grown to a high degree of perfection.

Third, if a crystal is to operate under a high incident power load, such as at a synchrotron insertion device beamline, it must combine high thermal conductivity with low thermal expansion so that the crystal can easily transfer heat to a cooling system and resist cracking caused by thermal gradients. Often, though not always, these parameters improve if the crystal is cooled by liquid nitrogen. The failure of YB_{66} to become widely used at synchrotrons, despite its favourably large *d*-spacings for 1–2 keV X-rays and its stability under irradiation, is due to its very poor thermal conductivity of 0.02 W cm^{-1} K^{-1} at 300 K, which drops even further at lower temperatures (Slack *et al.*, 1971). The contrasting success of silicon in monochromators exposed to high heat loads is due to silicon's combination of a zero in thermal expansion close to 125 K (Lyon *et al.*, 1977) with a high, isotropic thermal conductivity of 6.0 W cm^{-1} K^{-1} at that temperature. Since the thermal conductivity of silicon is 2.5–4 times better than that of germanium from 20 to 300 K (Glassbrenner & Slack, 1964), silicon has entirely supplanted germanium in synchrotron monochromators that receive X-ray beams from insertion devices. Diamond's thermal conductivity is over 10 W cm^{-1} K^{-1}, specimen-dependent but even better than that of silicon (Berman *et al.*, 1975), but remains little used because of the difficulty of growing single perfect crystals larger than a few cubic millimetres, as well as its extreme hardness. In crystals with non-cubic lattices, one may expect the thermal expansion and conductivity to be dependent on direction. A good example is the trigonal crystal quartz, whose thermal properties differ along the *a* and *c* axes of its hexagonal unit cell. Kosinski *et al.* (1992) provide thermal expansion coefficients at 293 K of 13.55×10^{-6} and 7.43×10^{-6} K^{-1} along the *a* and *c* axes, respectively. These are significantly higher than the corresponding value for silicon, 2.56×10^{-6} K^{-1} at 295.5 K (Deslattes *et al.*, 1980). Recommended values of thermal conductivity for quartz at 300 K are quite poor at 0.0621 and 0.104 W cm^{-1} K^{-1} along the *a* and *c* axes, respectively; these improve somewhat to 0.279 and 0.54 W cm^{-1} K^{-1} at 80 K (Touloukian *et al.*, 1970).

Fourth, the temperature dependence of the Bragg reflections of a crystal becomes important if the energy calibration needs to be precise. It also helps determine the range of X-ray energies that a crystal can diffract with reasonable efficiency. Temperature affects the Bragg reflections in three ways. First, thermal expansion changes the lattice parameters and therefore the *d*-spacing of the diffracting planes, altering the parameters in Bragg's law (equation 1). Second, the coordinates of the atoms within the unit cell may change with temperature. This does not occur in diamond, silicon or germanium, but it has been observed in quartz (Kihara, 1990) and it affects the calculation of the structure factor (equation 2). Finally, as temperature increases, the so-far neglected thermal motion of the atoms of the crystal increases with it. Crystals whose thermal properties are isotropic can be characterized by their X-ray Debye temperatures (which may differ from the Debye temperatures used in specific heat calculations). A higher X-ray Debye temperature corresponds to less thermally induced atomic motion at a given temperature and hence less decrease of the thermally averaged structure factor with increasing scattering vector. Diamond,

Table 1

Chemical formulas, symmetry and unit-cell dimensions of crystals commonly used as X-ray monochromators and analysers in EXAFS studies.

Unit-cell dimensions are given with their uncertainties (in parentheses) and first non-significant digits (as subscripts) where available. Temperatures are also given for the unit-cell dimensions where the sources provide them.

Material	Chemical formula	Crystal system	Space group	Unit-cell dimensions (room temperature)
Silicon	Si	cubic	$Fd\bar{3}m$	a = 5.431020511 (89) Å (NIST, 2018), consistent with other sources at 300 K†
Germanium	Ge	cubic	$Fd\bar{3}m$	a = 5.658 Å at 300 K‡
Diamond	C	cubic	$Fd\bar{3}m$	a = 3.567 Å at 300 K§
Quartz	SiO_2	trigonal	$P3_121$ or $P3_221$¶	a = 4.9137 (8), c = 5.4047 (12) Å at 298 K (Kihara, 1990)
Sapphire	Al_2O_3	trigonal	$R\bar{3}c$	a = 4.7590 (4), c = 12.99085 (22) Å at 287.35 K (Shvyd'ko & Gerdau, 1999)
Lithium niobate	$LiNbO_3$	trigonal	$R3c$	a = 5.148, c = 13.863 Å at 293 K (Hsu *et al.*, 1997)
Indium antimonide	InSb	cubic	$F\bar{4}3m$	a = 6.479 Å at 300 K‖
Lithium fluoride	LiF	cubic	$Fm\bar{3}m$	a = 4.0293 Å#
Beryl	$3BeO{\cdot}Al_2O_3{\cdot}6SiO_2$	hexagonal	$P6/mcc$	a = 9.21, c = 9.19 Å††
YB_{66}	YB_{66}	cubic	$Fm\bar{3}c$	a = 23.440 (6) Å (Richards & Kasper, 1969)
Topaz	$Al_2(F,OH)_2SiO_4$	orthorhombic	$Pbnm$ ‡‡	a = 4.6489 (24), b = 8.7935 (39), c = 8.3957 (39) Å at 298 K (Komatsu *et al.*, 2003)
Potassium acid phthalate	$CO_2HC_6H_4CO_2K$	orthorhombic	$P2_1ab$§§	a = 6.46_6, b = 9.60_9, c = 13.85_7 Å (Okaya, 1965)

† http://www.ioffe.ru/SVA/NSM/Semicond/Si/basic.html. ‡ http://www.ioffe.ru/SVA/NSM/Semicond/Ge/basic.html. § http://www.ioffe.ru/SVA/NSM/Semicond/Diamond/basic.html. ¶ α-Quartz exhibits two enantiomorphic forms, one in the space group $P3_121$ and one in $P3_221$, characterized by right-handed (3_1) and left-handed (3_2) screw axes. Confusingly, these two enantiomorphs are named laevo- and dextro-quartz, respectively. See Donnay & Le Page (1978) for a detailed discussion of the pitfalls of the quartz structure. ‖ http://www.ioffe.ru/SVA/NSM/Semicond/InSb/basic.html. # https://www.mindat.org/min-1749.html. †† https://www.mindat.org/min-819.html. ‡‡ $Pbnm$ describes a non-standard setting of the space group $Pnma$, No. 62 in *International Tables for Crystallography* Volume A (see Table 1.5.4.4 of Volume A). This non-standard setting results from the permutation of the three axes: the a, b and c axes of $Pnma$ become the c, a and b axes of $Pbnm$, respectively. §§ Similarly, $P2_1ab$ describes a non-standard setting of the space group $Pca2_1$, No. 29 in Volume A: the a, b and c axes of $P2_1ab$ become the c, a and b axes of $Pca2_1$, respectively.

silicon and germanium at room temperature have Debye temperatures of 1500–1880 K (Schoening & Vermeulen, 1969), 543 K and 290 K (Batterman & Chipman, 1962), respectively. Crystals that are more complex may have thermally induced vibrational amplitudes that depend strongly on direction, as is the case in quartz (Kihara, 1990). Crystals composed of more than one species of atom may have different Debye temperatures for different atoms. For example, sapphire (Al_2O_3) has an X-ray Debye temperature of 890 K for its Al atoms and 995 K for its O atoms (Lucht *et al.*, 2003). Crystals with low thermally induced atomic motion (high Debye temperatures) will more efficiently diffract X-rays at scattering vectors with large magnitudes $2\sin(\theta)/\lambda$.

Fifth, a crystal must be hard enough to resist plastic deformation, which would distort its lattice, but at the same time be soft enough to be cut, ground and polished. The hardness of a material can be characterized by several procedures. The Mohs hardness scale is simple, testing the ability of a material to be scratched by one of ten reference minerals from talc (Mohs hardness 1) to diamond (Mohs hardness 10). Other methods like the Knoop hardness test measure the width and depth of a mark left in a material by an indenter of standard shape subjected to a prescribed load.

A table of Bragg reflections of various crystals that have been used to study the absorption edges of a wide range of elements is printed in the *X-Ray Data Booklet* (Underwood, 2009). The values of $2d$ range from 1.624 Å for quartz ($50\bar{5}2$) to 26.632 Å for potassium acid phthalate (100). Table 1 provides the chemical formulas and lattice properties of a selection of these crystals and of several other crystals (diamond, lithium niobate, YB_{66}) that have been used on synchrotron beamlines. Table 2 provides the significant material properties (hardness, thermal expansion and conductivity, Debye temperature and method of manufacture) of all the crystals in Table 1 except potassium acid phthalate, for which data are not available. (It should be noted that potassium acid phthalate decomposes at 568 K and is an irritant. Crystals of this material are grown from slow evaporation from aqueous solutions.) Table 2 makes it clear that only diamond and sapphire could compete with silicon under high heat load, for only they have comparably high thermal conductivity and low thermal expansion, but they remain little used because it remains difficult to manufacture pure, dislocation-free crystals larger than a few mm^3, and because their extreme hardness makes them difficult to machine. Most of the other crystals must be kept away from high heat loads because of their poor thermal conductivity, particularly YB_{66}, which is the best suited for low-energy X-rays because of its large unit cell, but also has the lowest thermal conductivity of all the crystals listed in addition to being extremely hard.

4. Multi-crystal monochromators

4.1. Rocking curve and energy resolution for Bragg reflection from a single crystal

Bragg's law, given in equation (1), shows the particular wavelength that a single crystal can select in first order ($n = 1$) from a ray incident on the crystal at a specific grazing angle θ. However, because real beams have a finite divergence and bandwidth, the effect of small deviations $\Delta\theta$ and $\Delta\lambda$ from the central angle $\theta_{\rm B}$ and the central wavelength $\lambda_{\rm B}$ must be included when assessing a monochromator's suitability for a particular X-ray source. This effect is shown by taking the differential form of Bragg's law when $n = 1$:

$$\lambda_{\rm B}\cot\theta_{\rm B}\Delta\theta = \Delta\lambda. \qquad (3)$$

Table 2
Hardness, thermal expansion and conductivity, Debye temperature and preferred single-crystal manufacturing procedure for materials in Table 1.

Note: Details for potassium acid phthalate are not included in this table, as the relevant data are not available. Debye temperatures marked with an asterisk are X-ray values, which can be substantially lower than values determined by specific heat or elastic constants. RT = room temperature.

	Hardness					
Material	Mohs	Knoop (GPa)	Thermal expansion coefficient ($\times 10^{-6}$ K^{-1})	Thermal conductivity (W cm^{-1} K^{-1})	Debye temperature (K)	Preferred manufacturing method
Silicon	7	11.3†	2.33 (300 K), crosses zero at 120 K, −0.77 (80 K) (Gibbons, 1958)	1.56 (300 K), 13.9 (80 K) (Glassbrenner & Slack, 1964)	543* (Batterman & Chipman, 1962)	Floating zone
Germanium	6	7.65‡	5.75 (300 K), 1.05 (80 K) (Gibbons, 1958)	0.60 (300 K), 3.1 (80 K) (Glassbrenner & Slack, 1964)	290* (Batterman & Chipman, 1962)	Czochralski
Diamond (type I)	10	78–83 (Winchell, 1945)	1.07 (300 K), 0.023 (80 K) (Stoupin & Shvyd'ko, 2011)	9.0 (300 K), 35.3 (80 K) (Touloukian *et al.*, 1970)	1500–1880* (Schoening & Vermeulen, 1969)	High-pressure, high-temperature, chemical vapour deposition
Quartz	7	6.5–8.8 (Winchell, 1945)	13.55 (*a*, 293 K), 7.43 (*c*, 293 K) (Kosinski *et al.*, 1992)	0.0621 (*a*, 300 K), 0.104 (*c*, 300 K), 0.279 (*a*, 80 K), 0.54 (*c*, 80 K) (Touloukian *et al.*, 1970)	470 (Gray, 1957)	Hydrothermal (*Note*: piezoelectric)
Sapphire	9	16.7–21.6 (Winchell, 1945)	6.2 (*a*), 7.07 (*c*) at $T \gg 200$ K, ~0 at $T < 50$ K (Lucht *et al.*, 2003)	0.46 (300 K), 9.6 (80 K), ~200 (30 K) (Touloukian *et al.*, 1970)	890 (Al), 995 (O) (Lucht *et al.*, 2003)	Kyropoulos; for large specimens, heat exchanger method (Schmid *et al.*, 1994)
Lithium niobate§	5	5.2–8.8, strongly anisotropic (Brown *et al.*, 1975)	14.1 (*a*), 4.1 (*c*)	0.042 at 300 K	1118 (Li), 299 (Nb), 643 (O) (Etschmann & Ishizawa, 2001)	Czochralski (*Note*: piezoelectric)
Indium antimonide	3.8	2.2 (Madelung *et al.*, 2002)	5.04 at 300 K, changes sign at 55 K (Gibbons, 1958)	0.167 at 300 K (Busch & Steigmeier, 1961), ~1 at 55 K (Kosarev *et al.*, 1971)	203 (Madelung *et al.*, 2002)	Czochralski
Lithium fluoride	4	1.00 (Combes *et al.*, 1951)	37 at 283 K (Combes *et al.*, 1951)	0.113 at 314 K (Combes *et al.*, 1951)	732 (Browder *et al.*, 1991)	Bridgman or Kyropoulos (*Note*: poor thermal shock resistance)
Beryl	7.5–8.0	No data	2.6 (*a*), −2.9 (*c*) at RT (Morosin, 1972)	0.0435 (*a*), 0.0548 (*c*) at RT (Horai, 1971)	799 (Robie, 1988)	Hydrothermal
YB_{66}	No data	25.7 (Schwetz *et al.*, 1972)	4.8 at 373 K (Wong *et al.*, 1999)	0.02 at $T > 45$ K (Slack *et al.*, 1971)	1300 (Oliver & Brower, 1971)	Indirect-heating float zone (Wong *et al.*, 1999)
Topaz	8	12 (Winchell, 1945)	6.4 (*a*), 5.5 (*b*), 8.1 (*c*) at 298–1173 K (Komatsu *et al.*, 2003)	0.113 (mean) at RT (Horai, 1971)	910 (Tennakoon *et al.*, 2018)	Natural (*Note*: cleaves easily, handle with care)

† http://www.ioffe.ru/SVA/NSM/Semicond/Si/mechanic.html. ‡ http://www.ioffe.ru/SVA/NSM/Semicond/Ge/mechanic.html. § Material properties are taken from https://www.inradoptics.com/lithium-niobate unless otherwise noted.

Thus a single crystal introduces a correlation between the angle of incidence and the wavelength of the X-rays that it selects.

Equation (3) shows that the bandwidth of the selected beam is proportional to the incident beam's divergence. Some experiments, however, require a higher energy resolution than this condition permits. A theoretical limit to the energy resolution that can be achieved by a Bragg reflection from a single crystal is set by the width $\Delta\theta_{\rm rock}$ of the curve of diffracted intensity as a function of incidence angle θ (a 'rocking curve') when a monochromatic plane wave is incident on the crystal. The narrowest theoretically achievable energy resolution is then $\lambda_{\rm B} \cot\theta_{\rm B}\, \Delta\theta_{\rm rock}$. For a mosaic crystal, Zachariasen (1945) provides formulas for theoretical rocking curves under various approximate treatments of primary extinction (power loss of the beam crossing a single block caused by diffraction within it) and secondary extinction (power loss of the beam inside the crystal caused by diffraction in the blocks crossed by the beam before it reaches a particular block). The rocking curves of mosaic crystals are generally many times broader, have an integrated reflecting power many times greater, and have a peak reflectivity far lower than the rocking curves of perfect crystals. X-ray diffraction from perfect crystals must be treated using dynamical diffraction theory, which accounts for the coupling between the incident and the diffracted waves inside the crystal. The extinction of the beam within the crystal limits the beam's penetration depth even in the absence of absorption, thus giving the rocking curve a nonzero width. This is given by the so-called 'Darwin width' $\Delta\theta_{\rm D}$, which is approximately

$$\Delta\theta_{\rm D} = \frac{|P|\Gamma\left|F_H F_{-H}\right|^{1/2}}{(|b|)^{1/2}\sin 2\theta_{\rm B}} \qquad (4)$$

(Batterman & Cole, 1964). It is normally only a few arc-seconds. The quantities in this equation are as follows:

$P = 1$ if the beam's polarization is normal to the 'diffraction plane' (s-polarization) and $\cos 2\theta_{\rm B}$ if it is parallel to the 'diffraction plane' (p-polarization). The diffraction plane is spanned by $\mathbf{u}_0$, the unit vector along the incident beam, and $\mathbf{u}_H$, the unit vector along the diffracted beam.

$\Gamma = r_e\lambda^2/(\pi V)$, where r_e is the classical electron radius and V is the volume of the crystal's unit cell.

F_H and F_{-H} are the structure factors of the Bragg reflection along the reciprocal lattice vectors $\mathbf{H}$ and $-\mathbf{H}$, respectively.

$b = (\mathbf{n}\cdot\mathbf{u}_0)/(\mathbf{n}\cdot\mathbf{u}_H)$, where $\mathbf{n}$ is a unit vector normal to the crystal's surface. $b > 0$ if the diffracted beam emerges from the surface opposite the incident beam ('Laue case'). $b < 0$ if the diffracted beam emerges from the same surface struck by the incident beam ('Bragg case').

Bragg reflections from perfect crystals for which $|b| \neq 1$ are called 'asymmetric'. Though uncommon in EXAFS applications, they are notable because they change the width of the beam in the diffraction plane by a factor $1/|b|$ and the beam's divergence in the diffraction plane by a factor $|b|$.

The theoretical energy resolution can never be achieved with a single crystal because no real incident beam is a monochromatic plane wave. Also, a single crystal deflects the beam by an angle $2\theta_{\rm B}$, whereas it is generally more convenient, especially at synchrotron beamlines where space is restricted, to make the beam of selected X-rays parallel to the incident beam from the X-ray source. However, configurations of two

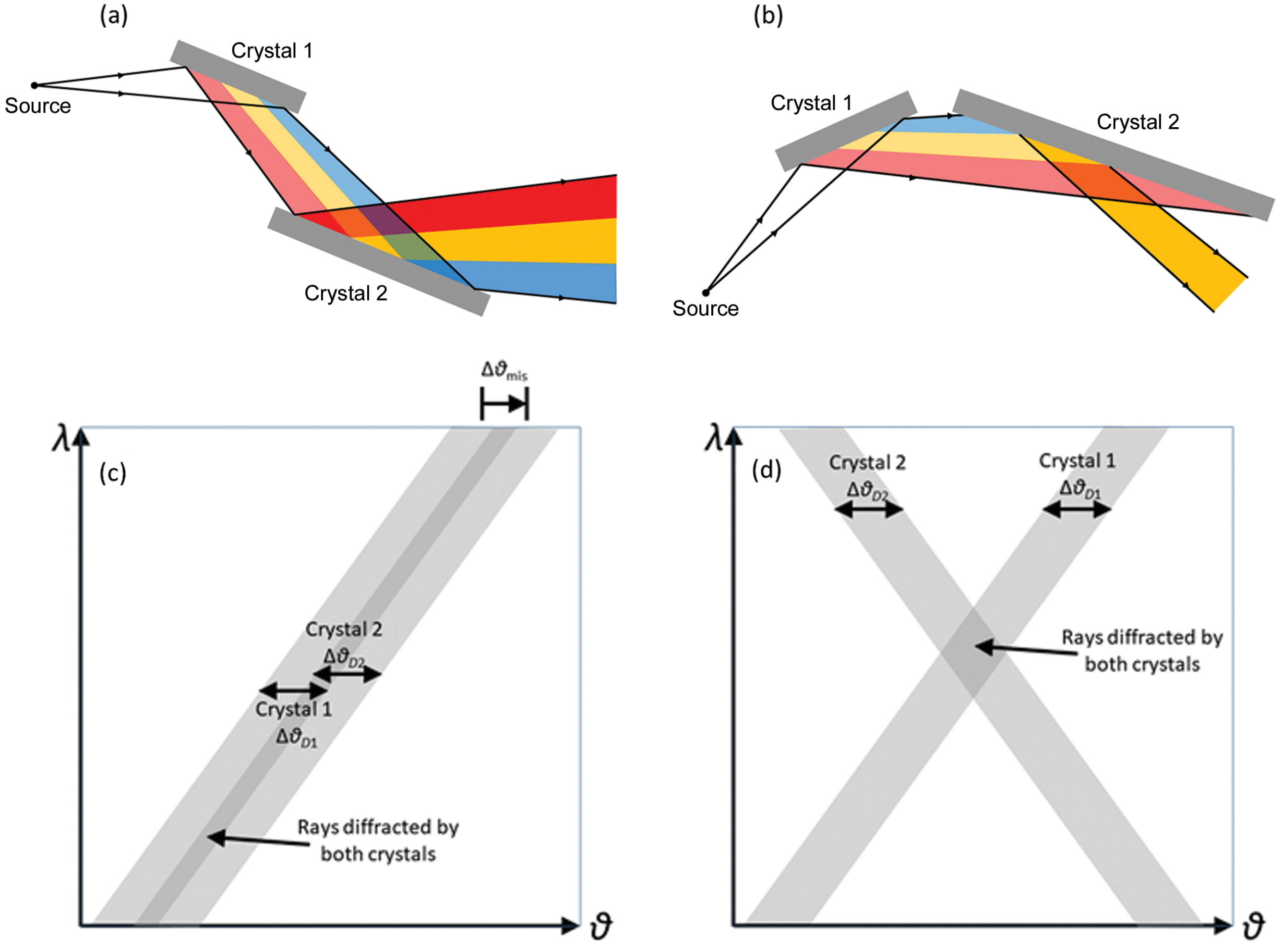

Figure 1
(*a*) Non-dispersive or (+−) double-crystal monochromator. (*b*) Dispersive or (++) double-crystal monochromator. (*c*) DuMond diagram for the non-dispersive monochromator in (*a*). (*d*) DuMond diagram for the dispersive monochromator in (*b*). For simplicity, both crystals are assumed here to be identical and perfect, as is normally true at synchrotron beamlines.

crystals can give the diffracted X-ray beam a more desirable set of properties, as will be shown below.

4.2. Double-crystal monochromators

In most cases, especially on synchrotron beamlines, it is convenient to choose two perfect crystals of the same material and oriented to the same Bragg reflection. Figs. 1(*a*) and 1(*b*) show the two ways in which two identical crystals can be arranged relative to each other when deflecting the beam in the same plane. In Fig. 1(*a*), the two crystals are parallel. Here, the beam deflection caused by the second crystal cancels out that caused by the first, so that the exiting beam is parallel to the entering beam. The crystals are then said to be in the (+−) or *non-dispersive* configuration. In Fig. 1(*b*), the beam deflection caused by the second crystal is in the same direction as that caused by the first. The crystals are then said to be in the (++) or *dispersive* configuration.

In the non-dispersive configuration, a ray leaving the first crystal at a sharper angle strikes the second crystal at a sharper angle too. On the other hand, in the dispersive configuration, a ray leaving the first crystal at a sharper angle strikes the second crystal at a shallower angle. This is reflected in the 'DuMond diagrams', the graphs of $\Delta\lambda$ against $\Delta\theta$ in Figs. 1(*c*) and 1(*d*) (DuMond, 1937). The first crystal is represented in each DuMond diagram by a grey band that follows the curve in equation (3). For small deviations $\Delta\lambda$ from λ_B and $\Delta\theta$ from θ_B, the band can be assumed to take the form of a line of slope $\lambda_B \cot\theta_B$. The width of this grey band along the $\Delta\theta$ axis is the width of the theoretical rocking curve, which for a perfect crystal is $\Delta\theta_D$ as shown in the figures. The second crystal is represented by a similar grey band, but in different ways depending on the configuration. In the non-dispersive configuration described in Fig. 1(*c*), the second crystal's grey band is parallel to that of the first crystal. If both crystals are exactly parallel, the two bands lie directly on top of each other, but if the second crystal is deviated by an angle $\Delta\theta_{\rm mis}$, the second crystal's grey band is shifted on the DuMond diagram by that amount along the $\Delta\theta$ axis. On the other hand, in the dispersive configuration described in Fig. 1(*d*), the second crystal's grey band is flipped horizontally. In both Fig. 1(*c*) and Fig. 1(*d*), the set of wavelengths and angles transmitted by the double-crystal monochromator is represented by the region where the grey bands of the two crystals overlap. Two important results emerge from this discussion:

Non-dispersive configuration: If the second crystal is rocked while the first crystal is held stationary, the measured rocking curve's width will depend only on the Darwin widths of both crystals, without any influence from the incident beam's divergence.

Dispersive configuration: The X-rays selected by this monochromator will have a divergence equal to the crystals' Darwin width and a correspondingly small bandwidth, independent of the divergence and bandwidth of the incident beam.

A more general treatment of double-crystal monochromators, including those with non-identical crystals and asymmetric Bragg reflections, may be found in Zachariasen (1945).

4.3. Channel-cut and constant offset ('fixed exit') double-crystal monochromators

The simplest double-crystal monochromator to manufacture and operate is the channel-cut monochromator. This is simply a single crystal with a groove of parallel sides cut through it, as shown in Fig. 2. The X-rays are diffracted first from one of the inner surfaces of the groove and then from the other in a non-dispersive configuration. The selected X-rays exiting the channel-cut monochromator are always parallel to the incident beam, being insensitive to both vibrations and misalignments of the channel-cut monochromator in roll and yaw. (See Fig. 2 for definitions.) However, while a channel-cut monochromator can be easily rotated to scan the selected photon energy of the exiting X-ray beam, the position of the exiting beam will vary in the process, as demonstrated in Figs. 2(*c*) and 2(*d*). This is a disadvantage if both the sample and the beam are small. Moreover, caution is advisable when using channel-cut monochromators, especially at synchrotron beamlines, for the following reasons:

(i) Because the first and second diffracting inner surfaces are rigidly fixed parallel to each other, harmonic wavelengths that satisfy Bragg's law in equation (1) at orders $n > 1$ will be transmitted along with the desired fundamental wavelength for which $n = 1$ as long as the higher-order reflections are permitted by the crystal's space group. This is not a serious problem when the source is a tube, which emits most of its X-ray intensity within the emission lines of the metal target. However, if the source is a synchrotron bending magnet or wiggler, the incident X-ray beam has a broad continuous

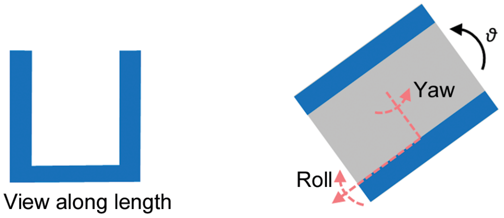

(a) View along length

(b) Rotation angles

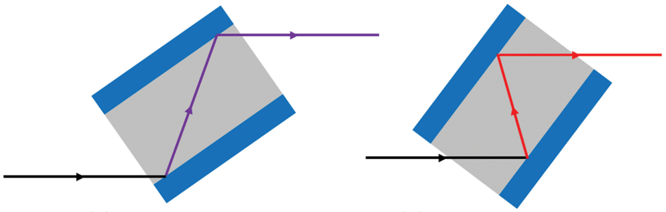

(c) High-energy setting

(d) Low-energy setting

Figure 2
Channel-cut monochromator. (*a*) View of channel-cut monochromator along its length. (*b*) Definitions of the rotation angles. The most important angle θ, which sets the Bragg angle, is marked in black. The roll and yaw, to which the channel-cut monochromator is much less sensitive, are marked with dotted lines. (*c*) Channel-cut monochromator at a low Bragg angle, which selects X-rays of high energy. (*d*) Channel-cut monochromator at a high Bragg angle, which selects X-rays of low energy. Notice the difference in the exiting beam's position.

bandwidth, and if the source is a synchrotron undulator, the incident X-ray beam has a spectrum consisting of a fundamental and harmonics determined by the undulator gap. In both cases, harmonics will be transmitted, with deleterious effects on the experimental background. This is not always a serious problem because harmonic rejection mirrors can often be used to reduce the intensity of the harmonics to an acceptable level. However, if the beamline is too short to allow the installation of additional mirrors, the harmonics may reach all the way to the sample.

(ii) If the incident beam on the first diffracting surface of the channel-cut monochromator has a broad bandwidth and high power, as is usual at synchrotron beamlines, it will raise the temperature of the area on that surface that it illuminates, thus distorting the crystal lattice there. The X-rays selected by the first surface, which carry only a small fraction of the original incident power, will then no longer exactly satisfy Bragg's law on the second surface, which remains largely free of thermal distortion. The photon intensity transmitted through the channel-cut monochromator will thus fall considerably below the ideal theoretical value.

(iii) The initial orientation of a channel-cut monochromator in a beam of broad continuous bandwidth, such as would be emitted by a synchrotron bending magnet or wiggler, can be tricky because Bragg reflections other than the one desired will always be excited, since the first diffracting surface will scatter the X-rays into a Laue pattern according to their wavelength. Different Bragg reflections cannot be distinguished by their deflection angle as with a single crystal because all the diffracted beams will emerge parallel to the incident beam. If the wrong Bragg reflection is chosen, the energy calibration will be incorrect. A slit must be placed downstream from the channel-cut monochromator to select the right Bragg reflection. The incident beam's cross section should not be large enough to cause the desired Bragg reflection's spot to overlap with the spots produced by any other Bragg reflections.

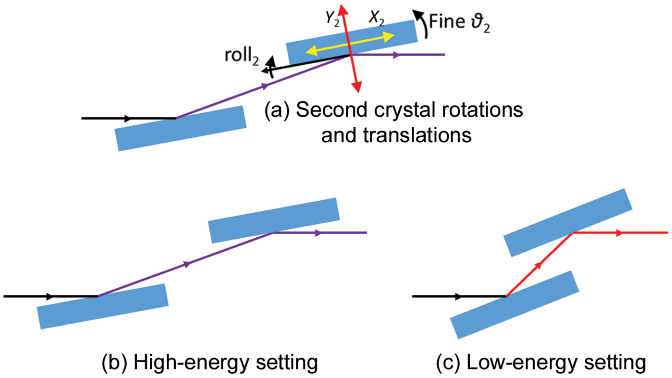

Figure 3

Fixed-exit monochromator. (*a*) Definitions of the angular and linear motions that are necessary to maintain the monochromator's performance. The subscript '2' means that these motions are applied to the second crystal only. (*b*) Fixed-exit monochromator at a low Bragg angle for selection of X-rays of high energy. (*c*) Fixed-exit monochromator at a high Bragg angle for selection of X-rays of low energy. Notice that the exiting beam's position is now independent of the X-ray energy selected.

(iv) On a single crystal, polishing with fine abrasive is often used to remove subsurface damage caused by sawing and grinding to the desired shape. However, a conventional polishing wheel cannot reach the inner surfaces of the channel-cut crystal that diffract the X-rays. A finger coated with abrasive would still not be able to polish these surfaces all the way down to the bottom of the groove, and could introduce unwanted surface texture because it is more difficult to move the finger along the depth of the groove than along its length. Therefore, unless the channel-cut monochromator is thoroughly etched to remove the damaged layers near the surfaces of the groove, the energy resolution may be significantly broadened beyond that expected from a perfect crystal. The need for an effective etchant that can reach the inner surfaces of the groove limits the potential choice of materials. Silicon and germanium crystals are amenable to being shaped into channel-cut monochromators because they can be effectively and isotropically etched by aqueous solutions of HF and HNO_3. Diamond crystals, on the other hand, are not amenable because they resist all acids and because the inner surfaces of the groove cannot be accessed by plasmas or reactive ions.

All of these problems can be solved by using a monochromator composed of two separate crystals arranged nondispersively. Normally, for simplicity of operation, the two crystals are mounted to a common rotation axis that sets the Bragg angle of both simultaneously. The diffracting surface of the first crystal is usually positioned on the common Bragg rotation axis. This design simplifies the construction of the cooling elements attached to the first crystal by minimizing the crystal's motion during energy scans. In the simplest design, the second crystal may be kept fixed with respect to the first crystal, except for fine angular adjustments that will be explained below. In addition, linear motions may be added to the second crystal to keep it in the beam over a wide energy scan, as shown in Fig. 3(*a*). The linear motions can be chosen to keep the exiting X-ray beam stationary as the Bragg angle is varied, as shown in Figs. 3(*b*) and 3(*c*). Such a 'fixed-exit' monochromator is an advantage in EXAFS experiments that require wide energy scans on a small sample.

Of course, a design composed of two separate crystals is more complex to build and has more stringent mechanical requirements than a channel-cut monochromator:

(i) Care must be taken to ensure that the roll angles of the two crystals are parallel; otherwise, the exiting X-ray beam will shift perpendicular to the diffraction plane during an energy scan. Generally, one of the two crystals will be given a motorized roll adjustment [see Fig. 3(*a*)], and the mutual roll alignment of the two crystals will be checked using an autocollimator before the monochromator chamber is closed. The final roll alignment is then adjusted in X-ray beam using the motorized roll stage.

(ii) This design is sensitive to vibrations, which may affect both the positions and the angles of both crystals separately, thus causing the beam at the sample position to waver.

On the other hand, a monochromator composed of two separate crystals offers several advantages over a channel-cut monochromator:

(i) The second crystal can be rotated independently of the first. Generally, the second crystal is provided with a fine piezoelectric angular stage for precise adjustment of its Bragg angle relative to the first crystal, as in Fig. 3(*a*). By setting the second crystal slightly away from exact parallelism with the first crystal ('detuning'), a user can reduce the transmitted harmonics while maintaining high intensity at the fundamental wavelength, taking advantage of the fact that higher-order reflections in perfect crystals generally have much smaller rocking-curve widths than the first-order reflection. In the same way, the second crystal's angle can be adjusted so that the X-rays selected by a thermally distorted first crystal fulfil Bragg's law on the second crystal. Thus the exiting beam can be maintained at a high photon flux. Some double-crystal monochromators, especially those at older or smaller synchrotrons where the electron beam current decays over time, maintain a steady harmonic level by adjusting this fine angular rotation through a feedback loop in which the exiting beam's intensity is the signal.

(ii) Each crystal can be individually polished on a conventional wheel to remove subsurface damage caused by machining. In this way, the highest possible energy resolution can be obtained.

(iii) The different *d*-spacing between the first and the second crystals due to the different heat loads that they cope with, especially in wiggler sources, can be accommodated by slightly changing the incident angle of the second crystal with respect to the first.

4.4. The fixed-exit dispersive four-bounce monochromator

Both the channel-cut and the fixed-exit monochromator are non-dispersive; therefore, the bandwidth of the exiting beam increases with the divergence of the incident beam. Because every real beam has some divergence, they never achieve the highest possible energy resolution. A dispersive monochromator can achieve this goal, but if built with only two crystals, it cannot keep the exiting beam's position fixed while its energy setting is scanned. Furthermore, if the incident beam is spread over a divergence much larger than the reflection's Darwin width, which for perfect crystals is generally only a few arcseconds, one can predict from the DuMond diagram in Fig. 1(*d*) that a dispersive monochromator will select only a tiny fraction of the incident intensity. Thus, high-resolution dispersive monochromators constructed from perfect crystals had low output when used with X-rays generated by X-ray tubes, which provide only low brightness over a wide angle. However, as soon as synchrotron X-ray sources began providing vastly increased intensity within much better collimated beams, Beaumont & Hart (1974) tested several dispersive monochromator designs that included more than two Bragg reflections. The simplest of these, and the only one that allows fixed exit, is a monochromator of four consecutive Bragg reflections in the (+−−+) arrangement shown in Fig. 4. This monochromator offers other advantages over double-crystal designs as well: variations in the source's angular position cause the beam on the sample to vary only in intensity but not in position, and the increased number of Bragg reflections improves the energy resolution by suppressing its tails.

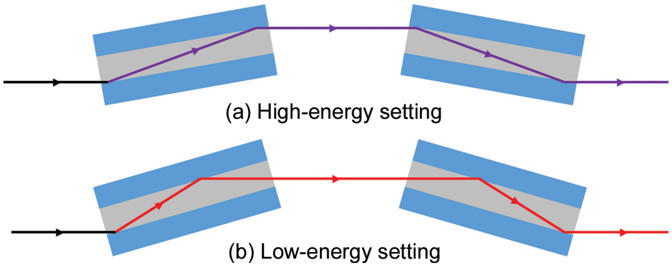

Figure 4
Four-bounce (+−−+) monochromator. (*a*) Low Bragg angle for selection of X-rays of higher energy. (*b*) High Bragg angle for selection of X-rays of lower energy.

Even this early work recognized the four-bounce (+−−+) monochromator's potential in EXAFS applications. However, the full development of a true energy-scanning perfect-crystal monochromator based on this design has taken many years, chiefly because proper scanning requires the first and second crystal pairs to be mounted on rotation axes that are stable, controllable and mutually synchronized, all within a few tenths of a microradian, in order to keep all crystals on the Bragg condition throughout. The important milestones are described by the references cited in Hayama *et al.* (2018), which describe earlier scanning monochromators installed on bending-magnet beamlines at BESSY II, NSLS, HASYLAB and LNLS in the 1980s and 1990s. The article itself demonstrates a successful (+−−+) scanning silicon (111) monochromator at beamline I20-scanning of the Diamond Light Source. The monochromator is able to maintain high output intensity without any external feedback or readjustment from 4 keV to 20 keV. The earlier scanning monochromators required only water cooling for the bending-magnet radiation, but the Diamond I20-scanning monochromator, being installed on a wiggler beamline that generates X-rays of much higher power spread over an equally large area, requires more challenging cryocooling with liquid nitrogen in order to keep the thermal distortion within acceptable levels.

4.5. Glitches

In wide energy scans taken by rotating the crystals of an X-ray monochromator, sharp dips in intensity will appear in the exiting beam when X-rays of certain specific energies are selected, as demonstrated in Fig. 5. These dips, called 'glitches,' are caused by the simultaneous excitation of Bragg reflections other than the principal one at the selected X-ray energy. Their positions in the energy scan depend on the incident beam's azimuthal angle, which is defined as the angle between the projection of the incident beam onto the main diffracting planes and a given reference direction parallel to the same planes. Therefore, although glitches cannot be avoided entirely over long energy scanning ranges, they can be kept away from certain especially desirable X-ray energies by adjusting the azimuthal angle, as done by Tang *et al.* (2015).

The analysis performed by Rek *et al.* (1984) and put into an accessible software package by Bowron (2012) can assist this part of the monochromator design. Libraries of glitches on specific perfect crystal monochromators, such as that provided by the Stanford Synchrotron Radiation Lightsource (1999), are publicly available.

The presence of glitches in the incident beam is nowadays not a problem in the majority of X-ray absorption spectroscopy (XAS) experiments when detectors with linear response are used and the sample is homogeneous, as they allow the cancellation of the glitches by normalizing with the incident intensity of the radiation.

However, there are some cases where, even when highly linear detectors are used, the presence of glitches in the incident beam affects the quality of the XAS data collected. This is the case when XAS measurements are taken on dilute solutions, whose weak X-ray fluorescence must be measured with a detector of large solid angle. In those cases, the non-fluorescent coherent and Compton scattering of the X-rays by the matrix of the sample adds a background that is superimposed on the collected sample fluorescence and has a differential scattering cross section dependent on the X-ray polarization. At synchrotron beamlines, the X-ray polarization is largely (though not completely) linearly horizontal. By placing the fluorescence detector so that it views the sample along the X-ray polarization vector, the non-fluorescent scattering is minimized, but because the detector has a finite solid angle, it cannot be completely removed. Moreover, evidently anything that alters the polarization state of the X-ray beam on the sample must also alter the spatial distribution of the collected non-fluorescent scattering. Sutter *et al.* (2016) found that indeed the appearance of a glitch changes not only the intensity but also the polarization of the X-ray beam. Studying the four-bounce silicon (111) monochromator at the Diamond Light Source EXAFS beamline I20-scanning, they found that the X-ray polarization may be rotated within a glitch by as much as 4.3°, in agreement with multiple-beam dynamical diffraction calculations. This makes the usual normalization of the fluorescence yield by the incident beam intensity increasingly ineffective as the sample grows more dilute. Improved normalization procedures that account for the polarization change remain to be developed.

5. Future developments

5.1. Vertical versus horizontal deflection

Crystal monochromators for X-rays at synchrotron beamlines are generally built to deflect the X-ray beam vertically. This is not a simple matter of taste, but is justified by the way modern synchrotrons operate. In current storage rings, the electron beam width and divergence are generally some 20–30 times larger in the horizontal plane than in the vertical plane. Standard double-crystal monochromators therefore transfer a narrow range of X-ray energies and thus achieve higher energy resolution if they deflect vertically, as can be seen from equation (3). For the same reason, the dispersive fixed-exit four-bounce monochromator selects a larger fraction of the incident X-ray intensity if it deflects vertically. The insertion of a collimating mirror upstream from the monochromator does not negate this advantage of vertical deflection. If the mirror is to collimate the beam horizontally, it must be longer in order to accept the greater horizontal divergence, and a larger residual divergence remains in the beam exiting the mirror because of the electron beam's greater horizontal width. All this will change with the forthcoming upgrade of many of the world's current synchrotron sources to diffraction-limited storage rings, in which the horizontal width and divergence of the electron beam will be greatly reduced so that they match the vertical width and divergence. Horizontally deflecting monochromators will then, in theory, perform as well as vertically deflecting ones, or even better because they can be

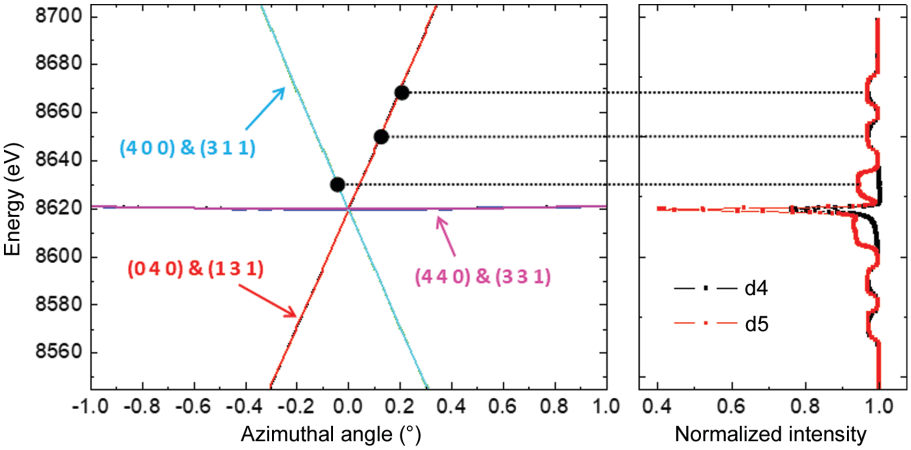

Figure 5
Sample of glitches measured in exiting beam from the Diamond Light Source I20-scanning silicon (111) four-bounce monochromator described by Hayama *et al.* (2018) in a typical energy scan. On the left is a plot of X-ray energies and azimuthal angles at which the labelled Bragg reflections can be excited simultaneously with the main 111 reflection (Bowron, 2012). On the right is a plot showing the measured glitches as a function of the selected X-ray energy. d4 is a diode detector located between the first and second pair of bounces. d5 is a diode detector just downstream from the last bounce. The solid circles connected to the glitches with dotted horizontal lines indicate the estimated azimuthal misorientation of the crystal that produced the glitch. An azimuthal angle of zero indicates that the incident beam lies in the plane of the [111] and [$11\bar{2}$] directions.

designed with greater stability against vibrations. Nanofocusing synchrotron X-ray beamlines, such as the Hard X-ray Nanoprobe I14 at Diamond Light Source, the Nanodiffraction beamline ID01 at the ESRF (Leake *et al.*, 2019), the X-ray Nanoprobe beamline 23A at the Taiwan Photon Source (Yin *et al.*, 2016) and the Sub-micron Resolution X-ray Spectroscopy beamline at NSLS-II (De Andrade *et al.*, 2011) have already applied horizontally deflecting double-crystal monochromators for their greater stability. However, the X-ray beams will still be mainly polarized in the horizontal direction, which for a horizontally deflecting Bragg reflection is p-polarization. The polarization factor P in equation (4) thus reduces the Darwin width of the Bragg reflection by a factor of $\cos 2\theta_{\rm B}$, and it also reduces the peak intensity of the rocking curve when the crystal is absorbing. Horizontally deflecting monochromators therefore will fail to transmit significant X-ray intensity if the Bragg angle is close to 45°.

The simultaneous need for cryogenic cooling, low mechanical strain in the crystals and high vibrational stability continues to challenge the achievement of optimal performance, especially on wiggler beamlines that generate high power densities over a wide area of the crystals. Crystal mounts must account for the different thermal contractions of juxtaposed materials during cooling and warming in order to avoid warping the crystal. Indium foils are often sandwiched between the crystals and their heat exchangers because they will deform plastically to fill gaps when pressure is applied and hence ensure a good thermal contact, but the effects of different loads and foil thickness on the thermal transfer efficiency and the mechanical strain of the crystal are imprecisely known. Bubbles or turbulent flow in the cooling medium can cause the crystals to vibrate and thus shift the beam position relative to the sample. Work on these issues is ongoing.

Acknowledgements

The author thanks Sofía Díaz-Moreno for critical reading of the manuscript.

References

Asadchikov, V. E., Butashin, A. V., Buzmakov, A. V., Deryabin, A. N., Kanevsky, V. M., Prokhorov, I. A., Roshchin, B. S., Volkov, Yu. O., Zolotov, D. A., Jafari, A., Alexeev, P., Cecilia, A., Baumbach, T., Bessas, D., Danilewsky, A. N., Sergueev, I., Wille, H.-C. & Hermann, R. P. (2016). *Cryst. Res. Technol.* **51**, 290–298.

Ashcroft, N. W. & Mermin, N. D. (1976). *Solid State Physics.* Philadelphia: W. B. Saunders Company.

Batterman, B. W. & Chipman, D. R. (1962). *Phys. Rev.* **127**, 690–693.

Batterman, B. W. & Cole, H. (1964). *Rev. Mod. Phys.* **36**, 681–717.

Beaumont, J. H. & Hart, M. (1974). *J. Phys. E Sci. Instrum.* **7**, 823–829.

Berman, R., Hudson, P. R. W. & Martinez, M. (1975). *J. Phys. C Solid State Phys.* **8**, L430–L434.

Bowron, D. T. (2012). *Monogli.* ISIS Neutron and Muon Source, Rutherford Appleton Laboratory, Didcot, UK.

Browder, J. S., Ballard, S. S. & Klocek, P. (1991). *Physical property comparisons of infrared optical materials*. In *Handbook of Infrared Optical Materials*, edited by P. Klocek, p. 179. New York: Marcel Dekker.

Brown, H., Ballman, A. A. & Chin, G. Y. (1975). *J. Mater. Sci.* **10**, 1157–1160.

Busch, G. & Steigmeier, E. F. (1961). *Helv. Phys. Acta*, **34**, 1–28.

Combes, L. S., Ballard, S. S. & McCarthy, K. A. (1951). *J. Opt. Soc. Am.* **41**, 215–222.

Cullity, B. D. & Stock, S. R. (2001). *Elements of X-ray Diffraction*, 3rd ed., Sections 4-4 to 4-6. New Jersey: Prentice Hall.

De Andrade, V., Thieme, J., Chubar, O. & Idir, M. (2011). *Proc. SPIE*, **8141**, 81410L.

Deslattes, R. D., Kessler, E. G., Sauder, W. C. & Henins, A. (1980). *Ann. Phys.* **129**, 378–434.

Donnay, J. D. H. & Le Page, Y. (1978). *Acta Cryst.* A**34**, 584–594.

DuMond, J. W. M. (1937). *Phys. Rev.* **52**, 872–883.

Etschmann, B. & Ishizawa, N. (2001). *Powder Diffr.* **16**, 81–85.

Gibbons, D. F. (1958). *Phys. Rev.* **112**, 136–140.

Glassbrenner, C. J. & Slack, G. A. (1964). *Phys. Rev.* **134**, A1058–A1069.

Gray, D. E. (1957). *American Institute of Physics Handbook.* New York: McGraw-Hill.

Hayama, S., Duller, G., Sutter, J. P., Amboage, M., Boada, R., Freeman, A., Keenan, L., Nutter, B., Cahill, L., Leicester, P., Kemp, B., Rubies, N. & Diaz-Moreno, S. (2018). *J. Synchrotron Rad.* **25**, 1556–1564.

Horai, K. (1971). *J. Geophys. Res.* **76**, 1278–1308.

Hsu, R., Maslen, E. N., du Boulay, D. & Ishizawa, N. (1997). *Acta Cryst.* B**53**, 420–428.

Ice, G. E. & Sparks, C. J. (1990). *Nucl. Instrum. Methods Phys. Res. A*, **291**, 110–116.

International Tables for Crystallography (2016). Volume A, *Space-Group Symmetry*, 6th ed., edited by M. I. Aroyo. Chichester: Wiley.

Källne, E. & Källne, J. (1983). *Phys. Scr.* **T3**, 185–190.

Kihara, K. (1990). *Eur. J. Mineral.* **2**, 63–77.

Komatsu, K., Kuribayashi, T. & Kudoh, Y. (2003). *J. Mineral. Petrological Sci.* **98**, 167–180.

Kosarev, V. V., Tamarin, P. V. & Shalyt, S. S. (1971). *Phys. Status Solidi B*, **44**, 525–534.

Kosinski, J. A., Gualtieri, J. G. & Ballato, A. (1992). *IEEE Trans. Ultrason. Ferroelect. Freq. Contr.* **39**, 502–507.

Leake, S. J., Chahine, G. A., Djazouli, H., Zhou, T., Richter, C., Hilhorst, J., Petit, L., Richard, M.-I., Morawe, C., Barrett, R., Zhang, L., Homs-Regojo, R. A., Favre-Nicolin, V., Boesecke, P. & Schülli, T. U. (2019). *J. Synchrotron Rad.* **26**, 571–584.

Lucht, M., Lerche, M., Wille, H.-C., Shvyd'ko, Yu. V., Rüter, H. D., Gerdau, E. & Becker, P. (2003). *J. Appl. Cryst.* **36**, 1075–1081.

Lyon, K. G., Salinger, G. L., Swenson, C. A. & White, G. K. (1977). *J. Appl. Phys.* **48**, 865–868.

Madelung, O., Rössler, U. & Schulz, M. (2002). Editors. *Indium antimonide (InSb), Debye temperature, density, hardness, melting point.* Landolt-Börnstein – Group III Condensed Matter 41A1β (Group IV Elements, IV-IV and III-V Compounds, Part b – Electronic, Transport, Optical and Other Properties). Berlin, Heidelberg: Springer-Verlag.

Morosin, B. (1972). *Acta Cryst.* B**28**, 1899–1903.

NIST (2018). *CODATA internationally recommended 2018 values of the fundamental physical constants*, https://physics.NIST.gov/cuu/Constants/index.html.

Okaya, Y. (1965). *Acta Cryst.* **19**, 879–882.

Oliver, D. W. & Brower, G. D. (1971). *J. Cryst. Growth*, **11**, 185–190.

Pattison, P., Suortti, P. & Weyrich, W. (1986). *J. Appl. Cryst.* **19**, 353–363.

Rek, Z. U., Brown, G. S. & Troxel, T. (1984). *Analysis and application of multiple diffraction phenomena in perfect crystal monochromators*. In *EXAFS and Near Edge Structure III*, Springer

Proceedings in Physics, Vol. 2, edited by K. O. Hodgson, B. Hedman & J. E. Penner-Hahn, pp. 511–513. Heidelberg: Springer.

Richards, S. M. & Kasper, J. S. (1969). *Acta Cryst.* B**25**, 237–251.

Robie, R. A. (1988). *Debye temperatures of selected silicate materials*. Department of the Interior, US Geological Survey, Open-File Report 88-663.

Sarker, A. (2016). *Mat. Res.* **19**, 505–512.

Schmid, F., Khattak, C. P. & Felt, D. M. (1994). *Am. Ceram. Soc. Bull.* **73**, 39–44.

Schoening, F. R. L. & Vermeulen, L. A. (1969). *Solid State Commun.* **7**, 15–18.

Schwetz, K., Ettmayer, P., Kieffer, R. & Lipp, A. (1972). *J. Less-Common Met.* **26**, 99–104.

Sergueev, I., Wille, H.-C., Hermann, R. P., Bessas, D., Shvyd'ko, Yu. V., Zając, M. & Rüffer, R. (2011). *J. Synchrotron Rad.* **18**, 802–810.

Shvyd'ko, Yu. V. & Gerdau, E. (1999). *Hyperfine Interact.* **123/124**, 741–776.

Slack, G. A., Oliver, D. W. & Horn, F. H. (1971). *Phys. Rev. B*, **4**, 1714–1720.

Stanford Synchrotron Radiation Lightsource (1999). *Monochromator Crystal Glitch Library*, https://www-ssrl.slac.stanford.edu/~xas/glitch/glitch.html.

Stoupin, S. & Shvyd'ko, Y. V. (2011). *Phys. Rev. B*, **83**, 104102.

Sutter, J. P., Boada, R., Bowron, D. T., Stepanov, S. A. & Díaz-Moreno, S. (2016). *J. Appl. Cryst.* **49**, 1209–1222.

Tang, Z., Zheng, L., Chu, S., Wu, M., An, P., Zhang, L. & Hu, T. (2015). *J. Synchrotron Rad.* **22**, 1147–1150.

Tennakoon, S., Peng, Y., Mookherjee, M., Speziale, S., Manthilake, G., Besara, T., Andreu, L. & Rivera, F. (2018). *Sci. Rep.* **8**, 1372.

Touloukian, Y. S., Powell, R. W., Ho, C. Y. & Klemens, P. G. (1970). *Thermophysical Properties of Matter: The TPRC Data Series*, Vol. 2, *Thermal Conductivity – Nonmetallic Solids*, pp. 174–182. New York: IFI/Plenum.

Underwood, J. H. (2009). *X-ray Data Booklet*, 3rd ed., Section 4, *Optics and Detectors*, Table 4-1. Compiled and edited by Albert C. Thompson. Berkeley: Lawrence Berkeley National Laboratory. Available online at http://xdb.lbl.gov/Section4/Sec_4-1.html.

Winchell, H. (1945). *Am. Mineral.* **30**, 583–595.

Wong, J., Tanaka, T., Rowen, M., Schäfers, F., Müller, B. R. & Rek, Z. U. (1999). *J. Synchrotron Rad.* **6**, 1086–1095.

Yin, G.-C., Chang, S.-H., Chen, B.-Y., Chen, H.-Y., Lin, B.-H., Tseng, S.-C., Lee, C.-Y., Wu, J.-X., Wu, S.-Y. & Tang, M.-T. (2016). *AIP Conf. Proc.* **1741**, 030004.

Zachariasen (1945). *Theory of X-ray Diffraction in Crystals.* New York: John Wiley & Sons.